Geomorphology 389 (2021) 107804

Contents lists available at ScienceDirect

Geomorphology

journal homepage: www.elsevier.com/locate/geomorph

A global landslide non-susceptibility map

Guoqiang Jia [a,b], Massimiliano Alvioli [c,*], Stefano Luigi Gariano [c], Ivan Marchesini [c], Fausto Guzzetti [c,d], Qiuhong Tang [a,b,**]

[a] Key Laboratory of Water Cycle and Related Land Surface Processes, Institute of Geographic Sciences and Natural Resources Research, Chinese Academy of Sciences, Beijing 100101, China
[b] University of Chinese Academy of Sciences, Beijing 100049, China
[c] Research Institute for Geo-Hydrological Protection, Italian National Research Council (IRPI CNR), via Madonna Alta 126, Perugia 06128, Italy
[d] Italian National Civil Protection Department, via Vitorchiano 2, Rome 00189, Italy

ARTICLE INFO

Article history:
Received 9 August 2020
Received in revised form 5 May 2021
Accepted 24 May 2021
Available online 1 June 2021

Keywords:
Non-susceptibility
Quantile non-linear model
Validation
Non-exposure analysis

ABSTRACT

At variance with conventional landslide susceptibility assessment, non-susceptibility analysis aims at selecting locations in which the likelihood of landslide occurrence is null or negligible. The advantage of this approach is that it does not require estimating different degrees of likelihood outside of the locations of negligible susceptibility. Thus, it entails the use of simplified classification methods. In this work, we tested and validated the existing non-susceptibility model with 18 global and regional landslide datasets, as a prior for the global application. The existing model was applied previously in Italy and the Mediterranean region, and defined by a non-linear relief vs. slope threshold curve, below which landslide susceptibility is negligible. Then, we applied a similar analysis, and proposed a global map, using relief and slope obtained from global elevation data at about 90-m resolution. The global map classifies 82.9% of the landmasses with negligible landslide susceptibility. The non-susceptible areas are broadly consistent with the “very-low” susceptibility class in existing global and continental landslide susceptibility maps and a national non-susceptibility map in the conterminous United States. Quantitative analyses revealed that population and settlements are denser within non-susceptible area than elsewhere, which makes the map of potential interest for non-exposure analysis, land planning and disaster responses at a global scale.

1. Introduction

Landslide hazard and risk assessment are a relevant scientific and social issue owing to the global impact of slope failures on human activities and natural environment. Recently, global landslide studies are becoming frequent, and efforts have been made to compile global landslide datasets and models applicable to global datasets (Kirschbaum et al., 2010, 2015; Froude and Petley, 2018; Haque et al., 2019). Global maps of landslide susceptibility (Hong et al., 2007a; Farahmand and Aghakouchak, 2013; Stanley and Kirschbaum, 2017), or global landslide hazard and risk assessment (Hong et al., 2006; Kirschbaum et al., 2009; Nadim et al., 2006, 2013) also exist. Rainfall thresholds for landslide initiation at a global scale were proposed (Guzzetti et al., 2008; Hong and Adler, 2008; Jia et al., 2020), as well as global landslide warning systems (Hong et al., 2007b; Kirschbaum and Stanley, 2018). A link between landslide features and climate change, mostly through rainfall data, at a global scale was also investigated (Kirschbaum et al., 2015; Gariano and Guzzetti, 2016; Haque et al., 2019). The reasons for a globally homogeneous landslide analysis are manifold, including: (a) it is useful in data scarce regions, where detailed information is not available (Jacobs et al., 2020); (b) it allows finding similarities and differences in the spatial pattern of landslide occurrence in different settings (Tanyas et al., 2019a, 2019b; Tanyas and Lombardo, 2020); and (c) it provides opportunities for different regions to communicate and compare their disaster prevention and mitigation strategies with a common baseline (Guzzetti et al., 2020).

Knowledge of landslide hazard requires the assessment of “where” landslides might occur or re-activate, “when” or how frequently they can happen, and “how large” they will be (Guzzetti et al., 2005; Alvioli et al., 2018). The first task entails landslide susceptibility analyses, i.e., the evaluation of landslide spatial occurrence. During past decades, a variety of landslide susceptibility analyses have been conducted at different scales with various mapping units, different geo-environmental conditions, and numerous methods and techniques (e.g., Guzzetti et al., 2005; Van Den Eeckhaut et al., 2012; Alvioli et al., 2016; Stanley and Kirschbaum, 2017).

* Corresponding author.
** Correspondence to: Q. Tang, Key Laboratory of Water Cycle and Related Land Surface Processes, Institute of Geographic Sciences and Natural Resources Research, Chinese Academy of Sciences, Beijing 100101, China.
E-mail addresses: massimiliano.alvioli@irpi.cnr.it (M. Alvioli), tangqh@igsnrr.ac.cn (Q. Tang).

https://doi.org/10.1016/j.geomorph.2021.107804
0169-555X/

The aim of landslide susceptibility analyses is to assign different likelihoods for landslide occurrence, and classify different spatial locations in different susceptibility levels. Recently, some authors prepared systematic reviews on global and regional landslide susceptibility analyses, and highlighted their definitions, methods, model evaluations, achievements and limitations (e.g., Budimir et al., 2015; Huang and Zhao, 2018; Reichenbach et al., 2018). Practical uses of susceptibility analyses are often limited by large uncertainties and inconsistencies of various input data, and difficulties to understand the different susceptibility maps based on numerous methods (Reichenbach et al., 2018).

On the other hand, a few authors considered “non-susceptibility” analyses, consisting in identifying areas where the probability of landslide occurrence is negligible or null. Godt et al. (2012) first proposed a threshold-based method to define areas with negligible likelihood of landslide occurrence, further defined as non-susceptible areas by Marchesini et al. (2014). These statistically based non-susceptibility analyses establish a morphometric threshold by using geographically consistent data, and provide a simple and practical way to determine non-susceptible areas by using only morphometric information and accurate landslide data. Compared with susceptibility analysis, non-susceptibility modeling reduced the uncertainties from input data and methods.

Non-susceptible areas are landslide-safe areas. Overlaying non-susceptibility and population or settlement maps provides a way to illustrate the portion of population or settlements that are not exposed to landslide occurrence (Marchesini et al., 2014), and it provides strategies for decision-making in land planning and disaster mitigation. Moreover, Godt et al. (2012) highlighted a potential application of non-susceptibility maps as a proxy for landslide susceptibility analyses by relating the “not non-susceptible” class with “moderate” or “high” susceptibility classes. This work provides such a tool in the global scale, using data available in a homogeneous way.

Both Godt et al. (2012) and Marchesini et al. (2014) assumed terrain slope and relief as key variables for selecting landslide non-susceptible locations, at pixel level. The key assumption of non-susceptibility analyses is that flat, low-relief regions are not prone to landslides, which is supported by the fact that topography is the main influencing factor in landslide susceptibility analysis (Dai et al., 2002; Hong et al., 2007a; Stanley and Kirschbaum, 2017; Broeckx et al., 2018). Since the model is data-driven, a standard procedure for performance evaluation is required. Godt et al. (2012) established their model based on five state inventories with wide spatial and temporal coverage and landslides of all types, and tested their proposed non-susceptibility map by comparing with previous susceptibility analysis in the conterminous United States. Marchesini et al. (2014) conducted model fitting, testing and comparison by using different landslide inventories and different statistical methods. Their work revealed a low false positive rate (*FPR*) of about 0.06 for the quantile non-linear (QNL) non-susceptibility model based on accurate and complete landslide inventories in Italy and Spain. The study obtained a well-validated non-susceptibility model.

Existing non-susceptibility analyses are focused on regional scales, i.e., in the conterminous United States (Godt et al., 2012), Italy and Mediterranean region (Marchesini et al., 2014), whereas many authors have worked on global landslide susceptibility (e.g., Nadim et al., 2006; Farahmand and Aghakouchak, 2013; Stanley and Kirschbaum, 2017). In their review of landslide susceptibility models, Reichenbach et al. (2018) recommended extending and further testing the “non-susceptible” terrain zonation in different geographical regions as to validate its applicability and serve as a proxy for global or regional landslide susceptibility and hazard assessment.

In this study, we first tested and validated the QNL model proposed by Marchesini et al. (2014) based on available global and regional landslide datasets. We used two global datasets, seven national datasets and nine regional datasets, and obtained relief and slope data from the ~90-m Shuttle Radar Topography Mission (SRTM) digital elevation model (DEM). We proposed a global landslide non-susceptibility map (GLNSM) based on the existing QNL model by Marchesini et al. (2014), and compared the proposed non-susceptibility map with existing global or continental susceptibility and non-susceptibility maps. Eventually, we estimated the global population size and settlement area not exposed to landslides as a potential application of this work. For further extending analyses of non-susceptibility, we investigated new QNL models for several regions and global models based on different landslide types.

2. Data

2.1. Topography data

The SRTM DEM is a quasi-global terrain elevation dataset, available between 60°N and 60°S latitude, and widely used in topographical information extraction. First released in 2003, version 4.1 is now available (https://srtm.csi.cgiar.org/srtmdata/; accessed on 18 December 2020; Jarvis et al., 2008). Existing non-susceptibility analyses were conducted based on SRTM DEM ~90-m data of version 2 (Marchesini et al., 2014), which is a “finished” product covering the global landmasses, but contains regions with missing data (Jarvis et al., 2008). The spatial accuracy of topographical information is of great importance for non-susceptibility analysis. In the new version of dataset, void pixels were filled with available high-resolution auxiliary regional DEMs and a series of interpolation techniques (Reuter et al., 2007).

In this study, we used DEM data of the latest version, with ~90-m resolution at the equator, in the original geographical (longitude and latitude) coordinate reference system (CRS, in WGS84, EPSG: 4326). Elevation data was used to calculate regional relative relief (R) and local terrain slope (S), the two morphometric variables used in the non-susceptibility model.

2.2. Landslide datasets

Landslide data is vital for calibrating and validating susceptibility and non-susceptibility maps. Despite widely present around the world, reported and mapped landslides are available only in part of the landmasses. Detailed landslide information with high accuracy and completeness is lacking (Guzzetti et al., 2012). The USA National Aeronautics and Space Administration (NASA) landslide team launched the Global Landslide Catalog (GLC), in which records are available with occurrence dates and locations, types, triggers and estimates of location accuracy since 2007 (Kirschbaum et al., 2010, 2015). To improve the completeness of landslide dataset, NASA subsequently launched the Cooperative Open Online Landslide Repository (COOLR; Juang et al., 2019), which is a product of citizen science and original researches, containing landslide points and related alphanumeric records updated until August 2020 (https://gpm.nasa.gov/landslides/; accessed on 18 December 2020). To ensure the accuracy of the dataset, they added a measurement of location accuracy for each landslide event based on multiple sources. The Global Fatal Landslide Database (GFLD) is another global landslide dataset, listing landslides that caused deaths from 2004 to 2017, and including landslides triggered by different non-seismic causes, e.g., rainfall and human activities (Froude and Petley, 2018; Petley and Froude, 2019). The location accuracy in GFLD is estimated based on geographical units such as villages or states.

Regional landslide datasets are also available for some specific nations and areas. These datasets were compiled by detailed image interpretation (e.g., McKeon, 2016), disaster reports (e.g., YNDPMC, 2016), newsfeeds (e.g., Li et al., 2016), and partly aided by field surveys. In USA, the U.S. Geological Survey leads the landslide monitoring (USGS, 2020). Statewise landslide inventories are available in Arizona (Cook et al., 2016), Oregon (Burns and Madin, 2009), Utah (Elliott and Harty, 2010), Vermont (Clift and Springston, 2012) and Washington (Slaughter et al., 2017). Systematic information for landslide occurrence is obtained from geologic maps, aerial photo and imagery interpretation, and GIS/GPS tools. Some of records are even checked in field, whereas some are just searched and digitized via news or report sources. In Europe, there are pan-European cooperations in landslide hazard and risk assessment (Wilde et al., 2018), and landslide inventories are conducted in most of the countries (Van Den Eeckhaut and Hervás, 2012). However, the datasets are not publicly available. In Italy, inventory FraneItalia includes events occurring between 2010 and 2019 (v2.0; Calvello and Pecoraro, 2018). This catalog is an interpretation product of news, reports and other text-based sources, presenting the location accuracy with three confidence descriptors named as certain, approximated and municipality (available: https://data.mendeley.com/datasets/compare/zygb8jygrw/1/2; accessed on 18 December 2020). Ireland has a long history of landslide inventory development (Creighton, 2006). The latest version of Ireland national landslide dataset was derived from high-resolution aerial photo interpretation spanning from 2000 to 2010, with validation in field and a 3D visualisation system (McKeon, 2016). In Oceania, spatial information of the inventoried landslides was developed in Australia (Osuchowski and Atkinson, 2008) and New Zealand (Rosser et al., 2017). The Australian landslide database was recently updated in 2018, and firstly launched under collaborative efforts of the federal, state and local. A statewise inventory was also developed in Tasmania (Mazengarb and Stevenson, 2010). The majority of the information was sourced from national and state reports, news and other publications, and adjusted more accurately based on aerial photograph interpretation and mapping. The New Zealand landslide database (NZLD) is a combined inventory to hold a number of existing landslide datasets (Rosser et al., 2017). Some of the data sources were derived from aerial photo interpretation with high-quality control. However, the public dataset is shared with no accuracy information. In China, a comprehensive national landslide dataset was published based on official documents, news reports and existing web databases (Li et al., 2016). The measurement of location accuracy is lacking. In two provinces of China, Guangdong and Yunnan, landslide information of about twenty years is available in the printed yearbook of disaster prevention and mitigation (GDDPMC, 2016; YNDPMC, 2016). The uncertainty of the position can be measured with two descriptors: approximated (village or street) and municipality (town). In Turkey, a fatal landslide dataset was recently produced and the uncertainty of the location varies from district/village to city (Görüm and Fidan, 2021).

Uncertainties exist for landslide datasets, especially the occurrence location. One reason is resulted from accidental error from data sources and systematic error from geographical transformation (Guzzetti et al., 2012; Froude and Petley, 2018). Moreover, the typical characteristics for certain landslide types make it not easy to accurately locate their locations such as rapid landslides, which may occur quickly and travel in a long way. To ensure the accuracy of landslide data, preliminary analysis and selection were conducted. For example, data entries with location accuracy less than 1 km were chosen in COOLR and GFLD datasets. For regional databases with detailed data sources, records derived from imagery interpretation, GIS methods or field check were used, such as Australian, Oregon and Tasmanian datasets; for other datasets, landslide events were selected based on given position descriptors, such as Italian, Turkish, Guangdong and Yunnan datasets (the “certain” and “approximated” records were used). For NZLD, we selected landslides with detailed occurrence time, and discarded these with no occurrence time. Specifically, all the data entries were used for the Chinese dataset. Some of datasets (e.g., Ireland and Oregon datasets) are provided with both point and polygon landslide features, of which recorded landslide events are not exactly the same owing to the different data sources or mapping methods. Thus, both of them are used in our validation. All the datasets were projected in the WGS84 CRS (EPSG: 4326). Table 1 lists summary information of the landslide data used in this work, including two global datasets, seven national datasets and nine regional datasets, six of which include landslides mapped as polygons. Detailed location accuracy, landslide type and trigger information for each dataset are available in a supplement excel file. Fig. 1 shows the administrative geographic extent of national and regional datasets (a global view and four regional views).

2.3. Landslide susceptibility and non-susceptibility maps

Whereas non-susceptibility represents zero or negligible likelihood of landslide occurrence, susceptibility classes represent well-defined intervals of likelihood of landslide occurrence in conventional susceptibility maps. To show a link between the two types of analyses, we compared non-susceptibility in GLNSM with the lowest susceptibility class in existing global and continental susceptibility maps. During the two past decades, large-scale susceptibility analyses have been widely prepared in Europe, Africa, and the world. Early global susceptibility maps were proposed by Nadim et al. (2006) and Hong et al. (2007a). In this study, we used three updated global susceptibility/risk maps proposed by Giuliani and Peduzzi (2011), Stanley and Kirschbaum (2017) and Lin et al. (2017), and two continental maps published by Broeckx et al. (2018) and Wilde et al. (2018) for Africa and Europe, respectively. All the above susceptibility maps show five classes (very low, low, moderate, high, and very high susceptibility), although the methods and criteria to define them are different across different studies.

In the conterminous United States, Godt et al. (2012) proposed a national landslide non-susceptibility map based on a general linear model (GLM; $S_{90} = 0.19R_{90} - 0.16$, $6^\circ \le S_{90} \le 21^\circ$), in which R_{90} and S_{90}

Table 1
Summary information of global (1–2), national (3–9) and regional (10–18) landslide datasets. Region: the geographical extent of datasets, the two global datasets are labeled by the name of datasets. Type: features of landslide data. Record (O): number of landslide records in the original datasets. Record (S): selected number of landslide records with high accuracy in each dataset. Area: area of region, from wiki pages (accessed on December 18, 2020). N_L: number of landslide records per 10^3 km^2.

#	Region	Extent	Type	Record(O)	Record(S)	Area (10^3km^2)	10^3N_L (km^{-2})	Reference
1	COOLR	global	point	12,685	3377	–	–	Juang et al., 2019
2	GFLD	global	polygon	5490	297	–	–	Petley and Froude, 2019
3	Australia	national	point	1974	274	7692	0.04	Geoscience Australia, 2012
4	China	national	point	990	815	9597	0.08	Li et al., 2016
5	Ireland	national	point	2778	855	84	10.18	McKeon, 2016
6	Ireland	national	polygon	1417	736	84	8.76	McKeon, 2016
7	Italy	national	point	4934	3195	301	10.61	Calvello and Pecoraro, 2018
8	New Zealand	national	point	19,030	5789	268	21.60	Rosser et al., 2017
9	Turkey	national	point	389	317	783	0.40	Görüm and Fidan, 2021
10	Arizona, USA	regional	polygon	6374	3717	295	12.60	AGS, 2015
11	Guangdong, China	regional	point	1491	781	180	4.34	GDDPMC, 2016
12	Oregon, USA	regional	point	13,994	2807	98	28.64	Burns and Madin, 2009
13	Oregon, USA	regional	polygon	44,929	5957	98	60.79	Burns and Madin, 2009
14	Tasmania, Australia	regional	point	3266	764	68	11.24	Mazengarb and Stevenson, 2010
15	Utah, USA	regional	polygon	25,589	1722	220	7.83	UGS, 2018
16	Vermont, USA	regional	point	2731	352	25	14.08	Clift and Springston, 2012
17	Washington, USA	regional	polygon	45,297	7650	185	41.35	WGS, 2020
18	Yunnan, China	regional	point	453	203	394	0.52	YNDPMC, 2016

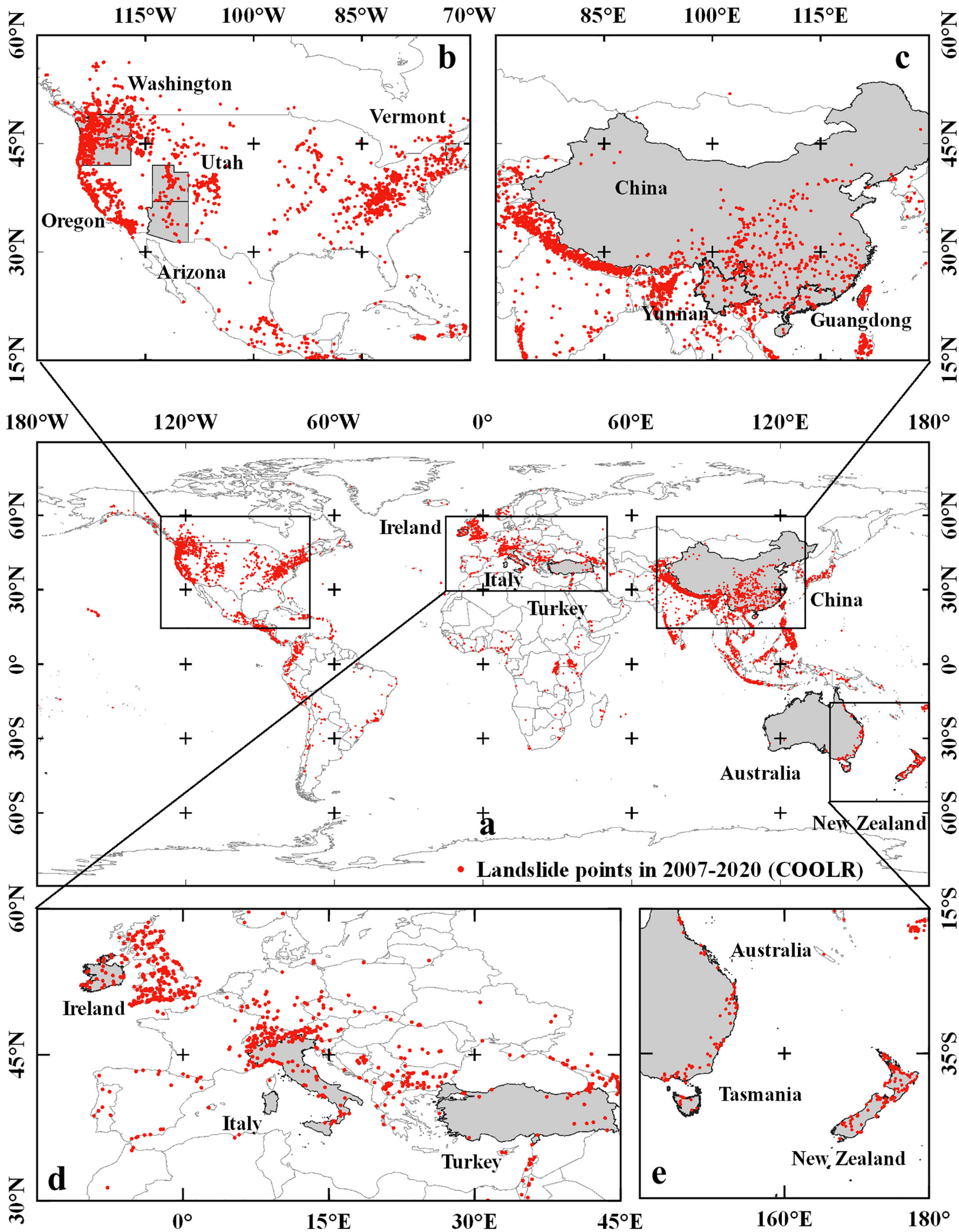

Fig. 1. Geographic (administrative) extents of available regional landslide datasets, of which six are national datasets labeled in a, in this analysis. Points in red represent landslide locations (12,685 points) in a global dataset (COOLR). Regional views (b-e) show four groups of the datasets.

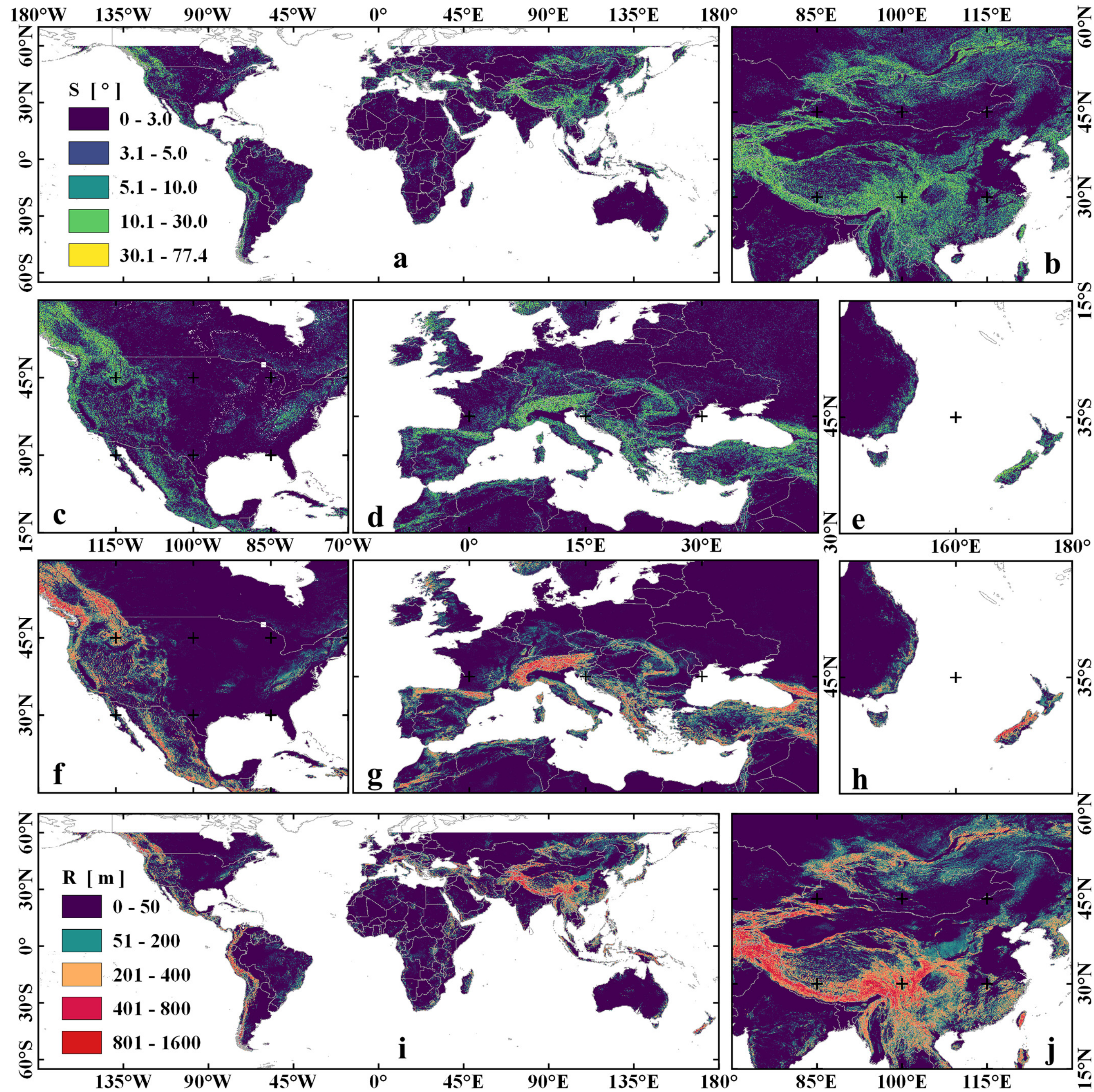

Fig. 2. Global maps of local terrain slope, *S* (a) and regional relative relief, *R* (i) based on the ~90-m SRTM DEM elevation data. Regional maps are shown to provide the enlarged views corresponding to that in Fig. 1, i.e., most of the Asia (b, j), most of the North America (c, f), Mediterranean region and its surroundings (d, g), and the eastern Australia and New Zealand (e, h).

represent the 90*th* percentiles of relief and slope values in each given landslide feature or pixel cell, respectively. Here we reconstructed the map based on the GLM model with slope and relief data prepared in our work to conduct a regional comparison with our global non-susceptibility map.

3. Methods

3.1. Non-susceptibility model

The existing landslide non-susceptibility model proposed by Marchesini et al. (2014) provided a minimum threshold curve of relief v.s. slope corresponding to historical landslide events. Below the threshold, landslide susceptibility is expected to be null or negligible, and thus non-susceptible areas are singled out. The QNL model performed best among all of the models considered by Marchesini et al. (2014) in terms of *FPR*. The analysis considered Italian high-quality regional landslide inventories, which were compiled through image interpretation and field campaigns between 1993 and 2013. The inventories contain almost all landslide types, and the majority of the landslides are rotational and translational slides, earth flows, complex, and compound movements according to the Cruden and Varnes (1996) classification scheme. The inventories cover most landslide-prone physiographical regions in Italy, which differ in lithological, climatic and land cover

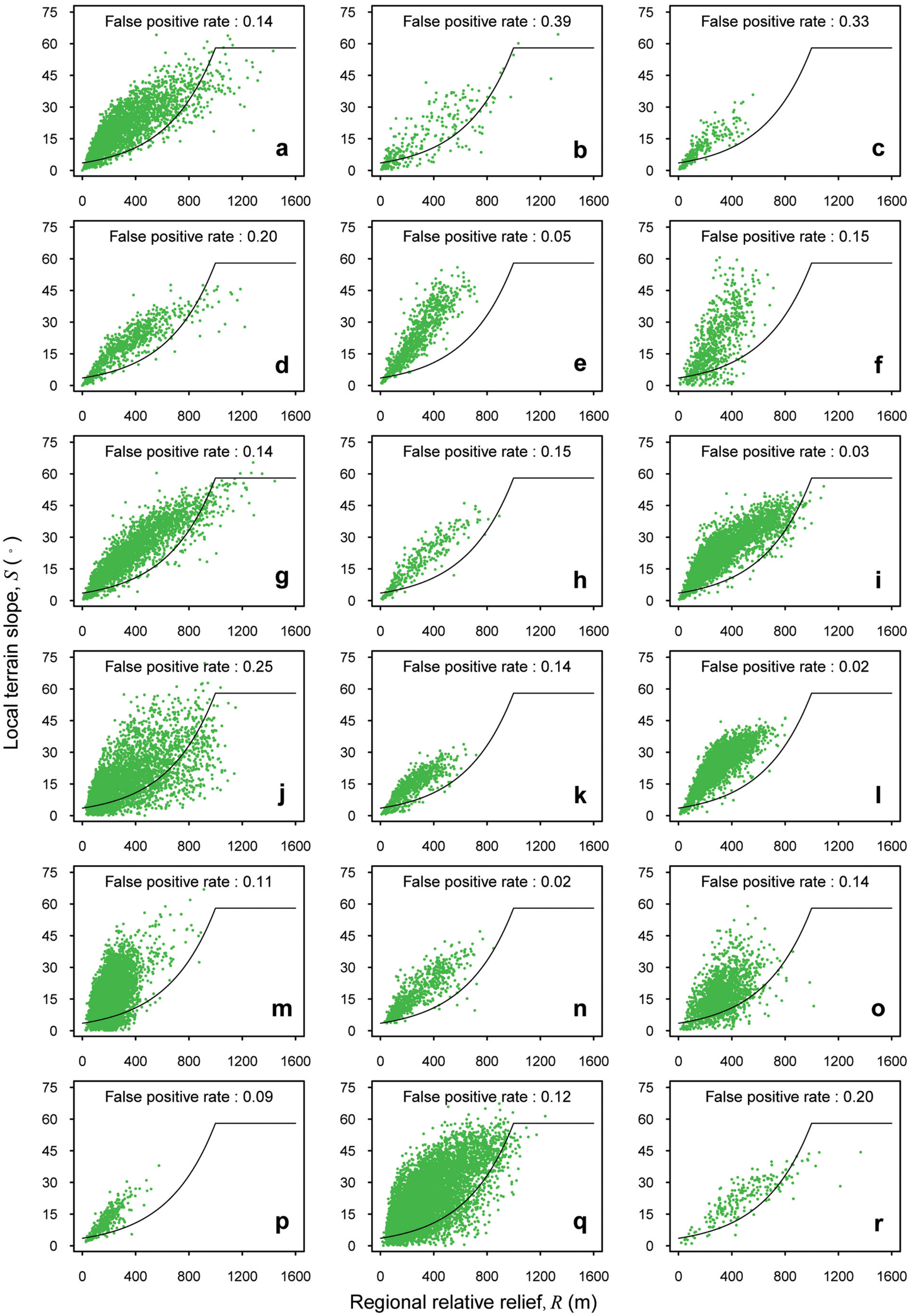
False positive rate : 0.14
a
False positive rate : 0.39
b
False positive rate : 0.33
c
False positive rate : 0.20
d
False positive rate : 0.05
e
False positive rate : 0.15
f
False positive rate : 0.14
g
False positive rate : 0.15
h
False positive rate : 0.03
i
False positive rate : 0.25
j
False positive rate : 0.14
k
False positive rate : 0.02
l
False positive rate : 0.11
m
False positive rate : 0.02
n
False positive rate : 0.14
o
False positive rate : 0.09
p
False positive rate : 0.12
q
False positive rate : 0.20
r
0
15
30
45
60
75
0
400
800
1200
1600
Local terrain slope, S (°)
Regional relative relief, R (m)

conditions (Guzzetti et al., 2012; Peruccacci et al., 2017; Alvioli et al., 2020). The QNL model was validated with an Italian national landslide inventory (Trigila et al., 2010), and a Spanish inventory. The QNL model is:

$$S = \alpha e^{\beta R}, \tag{1}$$

where S is the local terrain slope in degrees; R is the regional relative relief in meters, ranging between 0 and 1000 m; α=3.539 and $\beta = 0.0028$ are regression parameters. Eq. (1) represents the model's threshold: pixels whose representative point on the (R, S) plane falls below the curve are non-susceptible to landslide occurrence with 5% expected misclassifications. Validation of the model by Marchesini et al. (2014) revealed a *FPR* of 0.06 for all landslide types, ranging from 0.05 for translation and rotational slides to 0.21 for lateral spreads.

In this work, we tested the applicability of the data-driven QNL model proposed by Marchesini et al. (2014) for a worldwide application. The extrapolation of the model, from regional to global scale, indicates a large range of relief values (more than 1000 m), which was the validity range of the QNL model of Marchesini et al. (2014). Thus, we applied a maximum slope threshold of 58° (corresponding to the case when relief in the 15×15 window is equal to 1000 m in Eq. (1)), assuming areas with slope values over 58° as highly landslide-prone (Nadim et al., 2006; Hong et al., 2007a). A maximum slope threshold was also used in Godt et al. (2012). Moreover, we tried to propose new non-susceptibility models based on available landslide data for different regions and landslide types, to show their effects on non-susceptibility zonation.

3.2. Regional relative relief and local terrain slope calculation

Regional relative relief and local terrain slope are two basic inputs in landslide susceptibility and non-susceptibility analysis, and other branches of earth sciences. Marchesini et al. (2014) calculated S by elevation gradient within a 3×3-pixel moving window, and extracted R, the difference between maximum and minimum elevation, within a 15×15-pixel moving window. The aim of selecting different moving windows for two variables is to reduce their collinearity and capture the significantly different morphometric characteristics related to landscape evolution.

Pixel size difference at different latitudes was taken into account, for the calculation of slope, as follows. Firstly, the widths of each pixel cell in the longitude ($\delta x_{i,j}$) and latitude ($\delta y_{i,j}$) direction were calculated based on the geometry of the earth WGS84 ellipsoid; then the slope components in the longitude and latitude direction were defined by the partial derivatives of the polynomial to use most of elevation ($z_{i,j}$) information in a moving window, which are defined as follows:

$$\frac{\delta z_{i,j}}{\delta x_{i,j}} = \frac{(z_{i+1,j+1} + 2z_{i+1,j} + z_{i+1,j-1}) - (z_{i-1,j+1} + 2z_{i-1,j} + z_{i-1,j-1})}{8\delta x_{i,j}}, \tag{2}$$

$$\frac{\delta z_{i,j}}{\delta y_{i,j}} = \frac{(z_{i+1,j+1} + 2z_{i,j+1} + z_{i-1,j+1}) - (z_{i+1,j-1} + 2z_{i,j-1} + z_{i-1,j-1})}{8\delta y_{i,j}}, \tag{3}$$

Finally, the slope ($S_{i,j}$) in degree was obtained from its components in two direction.

$$S_{i,j} = \arctan\left(\left(\frac{\delta z_{i,j}}{\delta x_{i,j}}\right)^2 + \left(\frac{\delta z_{i,j}}{\delta y_{i,j}}\right)^2\right)^{1/2}, \tag{4}$$

Fig. 2 shows the global distribution of regional relative relief and local terrain slope, and highlights slope and relief values corresponding to the extent of landslide inventories in regional views (in Fig. 1), which also are relevant to most of the mountainous (Sayre et al., 2018) and landslide-prone regions (Froude and Petley, 2018).

3.3. Validation procedure

The proposed GLNSM map was validated with independent landslide datasets (in Section 2.2). For datasets containing polygon features, we overlaid the vector maps with the global relief and slope maps, and extracted the 90th percentiles (Godt et al., 2012) of relief and slope values in each polygon. We assumed the 90th percentiles of S and R values as corresponding to the landslide-triggering portion of the landslide body (Godt et al., 2012).

For each landslide dataset, we calculated the $FPR = FP / (FP + TN)$, where FP is the number of false positives, i.e., landslides below the R-S threshold of Eq. (1), and TN is the number of true negatives, i.e., landslides above the R-S threshold.

To consider the inherent uncertainties associated with the landslide locations in point datasets, we considered a circular 1-km buffer for each landslide point, and then conducted the same evaluation of *FPR* used for the polygon datasets. We further considered reactivations within a 1-km buffer as a single record in the landslide datasets, to avoid artificially increasing the values of *FP* or *TN* (Biasutti et al., 2016; Benz and Blum, 2019).

4. Results and discussions

4.1. Non-susceptibility model: validation against landslide datasets

For each landslide dataset (Table 1), we extracted morphological characteristics based on location information of landslides and plotted their relief and slope (Fig. 3). Based on the QNL non-susceptibility model, *FPRs* were calculated. Thirteen out of eighteen datasets have $FPR < 0.15$, and five have less than 10% of landslides located in non-susceptible areas ($FPR < 0.10$). Overall, we grouped the eighteen datasets into a single one, including all of the records. It turns out that about 12% of the landslides are located in non-susceptible areas (Table 2; in total, 39,608 individual landslides were considered). The percentage is lower for translational/rotational slides, earth flows ($FPR = 0.09$), and flows ($FPR = 0.05$). The results coincide with the good performances of QNL non-susceptibility model for translational/rotational slides and slow flows in Marchesini et al. (2014). By comparison, performance is poor for debris flows, mudslides and earth slides. Performance associated to rapid landslides is poor in Marchesini et al. (2014) as well. The reason may lie in the typical low slope associated to mudslides, and rapid development of debris flows, which can also travel into nearly flat areas (travel angle values can be also equal to 4°, Rickenmann, 2005). Moreover, rapid landslides are always triggered by heavy rain or huge fluctuations of earth owing to instantaneous strength loss (such as liquefaction of granular soils; Hungr, 2007). Thus, they could occur at lower slopes.

For global datasets, COOLR has a better match with the QNL model than GFLD. Fig. 3a and b, respectively, show a direct comparison on

Fig. 3. Validation results for available global and regional landslide datasets (Table 1). Green points represent the regional relative relief and local terrain slope corresponding to each landslide feature, and black curves the quantile non-linear (QNL) non-susceptibility threshold curve (Eq. (1)). Landslide datasets: (a) COOLR, (b) GFLD, (c) Australia, (d) China, (e) Ireland (point features), (f) Ireland (polygon features), (g) Italy, (h) Turkey, (i) New Zealand, (j) Arizona, USA, (k) Guangdong, China, (l) Oregon, USA (point features), (m) Oregon, USA (polygon features), (n) Tasmania, Australia, (o) Utah, USA, (p) Vermont, USA, (q) Washington, USA, (r) Yunnan, China. False positive rate (*FPR*) is the ratio of the number of landslides below the threshold curve (false positives, *FP*) over the total number of landslides (*FP* and true negatives, *TN*) in each dataset.

Table 2
Validation results of the proposed quantile non-linear (QNL) non-susceptibility model by Marchesini et al. (2014) for different landslide types based on all the landslide data of eighteen datasets (in Table 1). About 31% of the landslides include type information. False positives (*FP*): number of landslides below the QNL threshold curve (in non-susceptible area).

Landslide type	False positives (*FP*)	Total number of landslides (*TN* + *FP*)	False positive rate (*FPR*)
Flows	31	570	0.05
Falls	85	973	0.09
Slides	130	1197	0.11
Complex landslides	107	1029	0.10
Debris flows	271	1507	0.18
Earth flows	83	921	0.09
Translational/rotational slides	185	2079	0.09
Mudslides	90	773	0.12
Earth slides	763	3302	0.23
(undefined)	2884	27,257	0.11
Total	4629	39,608	0.12

the (R, S) plane of COOLR and GFLD datasets with the threshold of Eq. (1). In this case, the reason may lie in the fact that GFLD is a dataset containing only fatal landslides with lower overall representativeness and, most importantly, with a relative abundance of rapid landslides that typically cause more deaths due to their runouts extending on the flat areas.

In the case of regional datasets, Ireland, New Zealand, Oregon and Tasmania (Fig. 3e, i, l and n) have good performance, $FPR < 0.05$, while Australia and China (Fig. 3c and d) have poor performance, $FPR \geq 0.20$. We maintain that the non-susceptibility model works well with an overall low *FPR* and good performance.

Marchesini et al. (2014) highlighted the importance of accurate and complete landslide information for the non-susceptibility zonation. Here, we used the density of landslide events (N_L: number of landslide records per 10^3 km^2 for each dataset, in Table 1), as a proxy of completeness, exploring the relationship between N_L and *FPR*. Global datasets are excluded from this analysis, due to their manifest poor completeness. Fig. 4 indicates that a linear relationship exists between *FPR* and N_L. As N_L increases, *FPR* decreases, suggesting that high landslide density might improve the performance of validation. The reason of high *FPR*s in Australia, China and Arizona (Fig. 3c, d and j) probably lie in the poor completeness of landslide datasets. Further application of non-susceptible analyses requires more complete landslide datasets, and the number of reported landslides per area of Vermont (0.014 km^{-2}) could be a reference to assess the completeness of landslide inventories with an expected good *FPR* (less than 0.10 for point datasets and 0.17 for polygon datasets based on the linear relationships in Fig. 4b and c, respectively).

4.2. Global landslide non-susceptibility map

An overall good performance is illustrated for QNL model proposed by Marchesini et al. (2014) for available global and regional datasets in Section 4.1. Thus, we proposed a global landslide non-susceptibility map to show the distribution of landslide non-susceptible areas in ~90-m resolution (Fig. 5). The map indicates that 82.9% of global landmasses are located in non-susceptible areas, higher than the percentage of non-mountainous areas (69.5%; Sayre et al., 2018), suggesting that some of the mountainous areas are relatively stable. A further overlaying analysis reveals that GLNSM encompasses 80% of the global non-mountainous areas. Marchesini et al. (2014) quoted 63% for the percentage of non-susceptible areas in the Mediterranean region, which is expected, given that Mediterranean region is highly prone to landslide occurrence (Wilde et al., 2018). The corresponding percentages of non-susceptible areas are also low in Asia (74.8%) and North America (78.5%; Fig. 5a), corresponding to high fatal landslide incidence in the Southern, Eastern and Southeastern Asia, and Western North America (Froude and Petley, 2018). Regional views (Fig. 5 b-e) show low percentages of non-susceptible areas in the western United States, Italy, the eastern Australia, New Zealand, and the Himalayas, in agreement with landslide hotspots in previous studies (Kirschbaum et al., 2015; Haque et al., 2019).

As stated in Godt et al. (2012), landslide susceptibility maps are possible choices for testing the applicability of GLNSM. For available global and continental susceptibility maps in Section 2.3, the very-low class of each map was overlaid with our non-susceptibility map. The comparison revealed that worldwide 91.5% of the "very low" susceptibility pixels are located in non-susceptible areas, and specifically in the European susceptibility map and the global map proposed by Stanley and Kirschbaum (2017), more than 99% of the pixels classified with the very-low susceptibility are located in non-susceptible areas (Table 3).

We further compared the GLNSM with the national non-susceptibility map in the conterminous United States. Fig. 6 shows the two non-susceptibility maps in the region, based on the GLM and QNL models, respectively. The two maps share similar spatial distribution of non-susceptible areas. They almost hold the same pattern in the western and eastern USA, where high incidence of landslides exists. The two maps coincide with each other in about 80% of the area of the conterminous USA, while the map of GLM model (Fig. 6b) predicts less non-susceptible areas in the western and middle USA than that of QNL model, and the reverse in the eastern USA. The GLM model was established in a narrow interval, i.e., [6°, 21°], of local terrain slope and not validated with any landslide dataset. Actually, the slope values range from 0° to 71° in the conterminous USA (Fig. 2), and only about 25% of the landmasses has a local terrain slope in the interval of [6°, 21°]. Thus, large portion of the landmasses remains undefined within

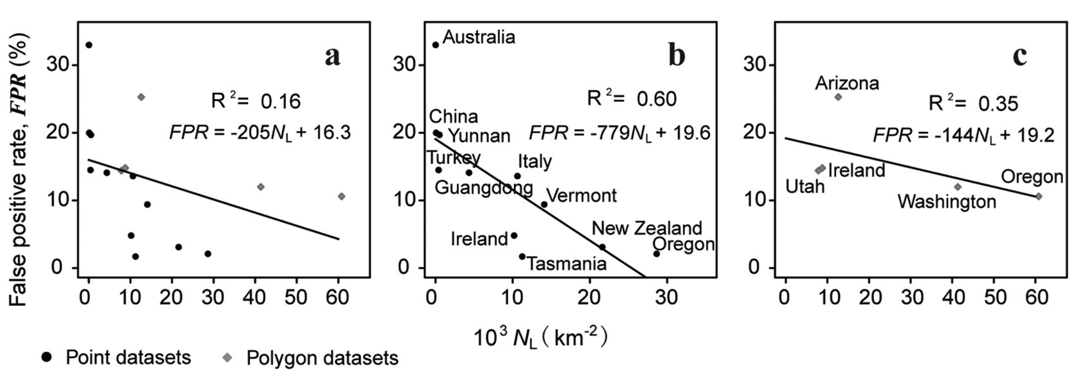

Fig. 4. Relationships between the landslide density (N_L represents the number of reported landslides per 10^3 km^2 in Table 1) and *FPR* for regional landslide datasets in Fig. 3: (a) point and polygon datasets, (b) point datasets, (c) polygon datasets. Black curves are linear fits.

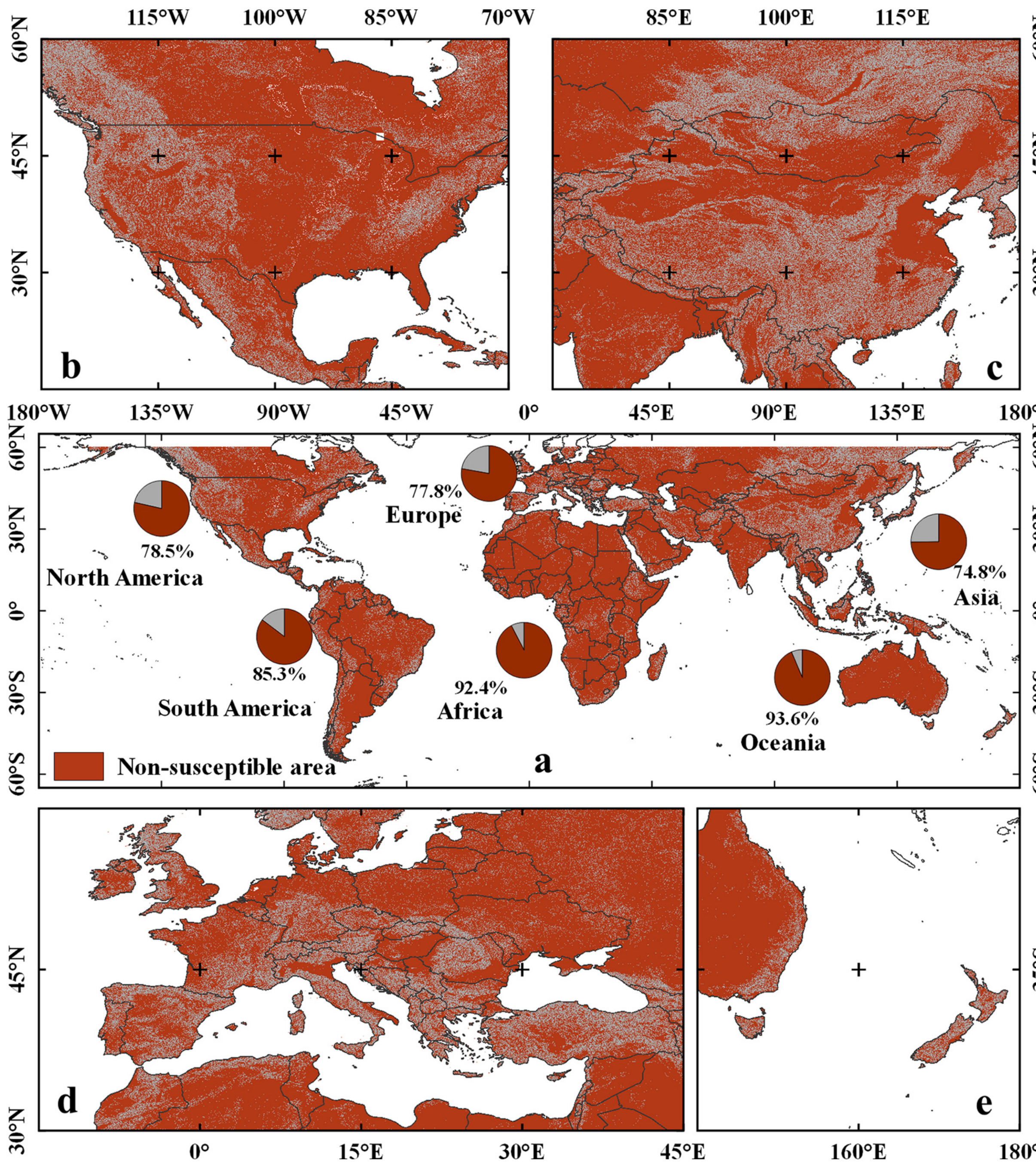

Fig. 5. A global map of landslide non-susceptibility in ~90-m resolution (a) based on QNL model proposed by Marchesini et al. (2014) in Section 3.1, and percentages of non-susceptible areas in each continent. Landmass outside the non-susceptible areas is shown in light gray. Non-susceptible areas are also mapped in regions corresponding to that in Fig. 1, i.e., most of the North America (b), most of the Asia (c), Mediterranean region and its surroundings (d), and the eastern Australia and New Zealand (e).

the GLM model. The above consideration partly explains the discrepancies between the two maps. The regional QNL model based on available USA state datasets reveals a lower *R-S* threshold compared with the QNL model by Marchesini et al. (2014) (see Section 4.4). Thus, further investigations are needed to conduct regional non-susceptibility analyses with more accurate and complete landslide inventories.

4.3. Relevance of the non-susceptibility map

Marchesini et al. (2014) conducted a non-exposure analysis to estimate sizes of settlement and population to possible landslide occurrence. The non-exposure outputs are relevant for decision-making in disaster prevention, land management and planning.

We conducted non-exposure analysis by using grid settlement data in 2014 and population data in 2015 with ~1-km resolution, available from the Global Human Settlement Layer Data Package (Florczyk et al., 2019). The human settlement data is a product derived from the Global Land Survey Landsat image, and the population data were disaggregated and resampled from the Gridded Population of the World provided by the Center for International Earth Science Information Network of Columbia University. Global overlay of these layers with the GLNSM reveals that 91.2% of built-up areas, and 91.8% of the

Table 3
Comparison between the lowest susceptibility class in global and continental susceptibility maps and non-susceptible class in our global landslide non-susceptibility map (Fig. 5a).

Extent	Susceptibility map	Non-susceptible area in "very low" class
Global	Giuliani and Peduzzi, 2011	86.0%
	Stanley and Kirschbaum, 2017	99.4%
	Lin et al., 2017	89.0%
	(Average)	91.5%
Africa	Broeckx et al., 2018	97.8%
Europe	Wilde et al., 2018	99.2%

Table 4
Statistics of population and human settlement in non-susceptible and "not non-susceptible" areas in a quasi-global scale.

	Not non-susceptible area	Non-susceptible area	Total
Area (10^6 km^2)	20.1	96.9	117.0
Percentage of area	17.1%	82.9%	100.0%
Built-up area (10^3 km^2)	67.5	701.3	768.8
Percentage of built-up area	8.8%	91.2%	100.0%
Built-up density	0.3%	0.7%	0.6%
Population (10^6)	594	6632	7226
Percentage of population	8.2%	91.8%	100.0%
Population density (km^{-2})	29.6	68.2	61.6

population are located in non-susceptible areas (Table 4), larger than the percentage of non-susceptible areas itself (82.9%; Table 2). The majority of people and buildings are located in relatively safe conditions, and the densities of built-up area and population size in non-susceptible areas are greatly larger (over two times) than those in "not non-susceptible" areas.

4.4. Regional and landslide type effects on non-susceptibility analysis

Whereas geological environments may influence the spatial pattern of landslide occurrence and failure mechanisms vary with landslide types (e.g., Jia et al., 2020), we try to establish QNL non-susceptibility models for different regions and landslide types as compared with the model proposed by Marchesini et al. (2014). We grouped the landslide datasets as four new datasets based on regional views in Fig. 1, and labeled as Region B (Fig. 1b), C (Fig. 1c), D (Fig. 1d) and E (Fig. 1e), respectively. A global model was also established based on the COOLR dataset. To establish models of different landslide types, we only considered the COOLR dataset to assure consistent landslide information. Here, debris flows, translational/rotational slides, mudslides, rock falls, complex landslides and others are considered.

Relief-slope thresholds in the globe and four regions (Fig. 7), for six landslide types (Fig. 8) are lower than the QNL model proposed by Marchesini et al. (2014) (denoted by Model_Ma). The minimum slope threshold values (α) for regions vary from about 1.2 to 3.7 (Table 5), less than that of Model_Ma except for Region E. The threshold curve of Region E (Fig. 7e; based on Australia, New Zealand and Tasmania datasets) is the closest to Model_Ma. Region C (Fig. 7c; based on China, Guangdong and Yunnan datasets) and D (Fig. 7d; based on Ireland, Italy and Turkey datasets) share the same scale value (β). There are big differences between the models of Region B (Fig. 7b; based on USA state datasets) and other models. Significant differences

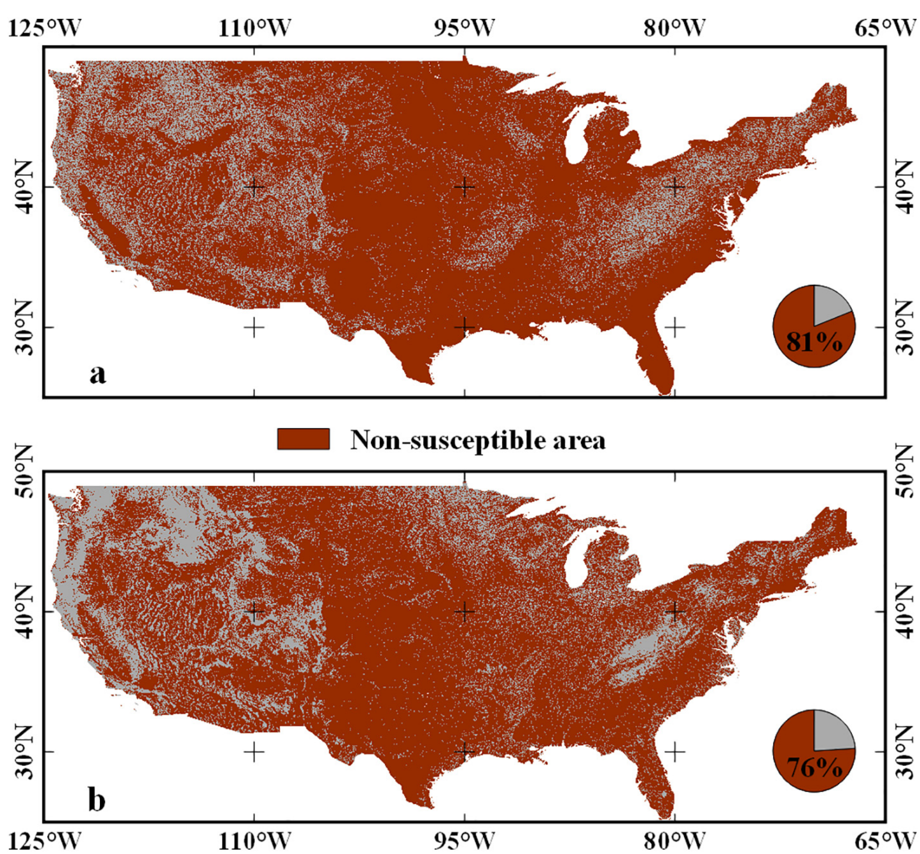

Fig. 6. Non-susceptibility maps (~90 m) in the conterminous United States based on the QNL model (a) proposed by Marchesini et al. (2014) and the linear model (b) proposed by Godt et al. (2012). Landmasses outside the non-susceptible areas is shown in light gray.

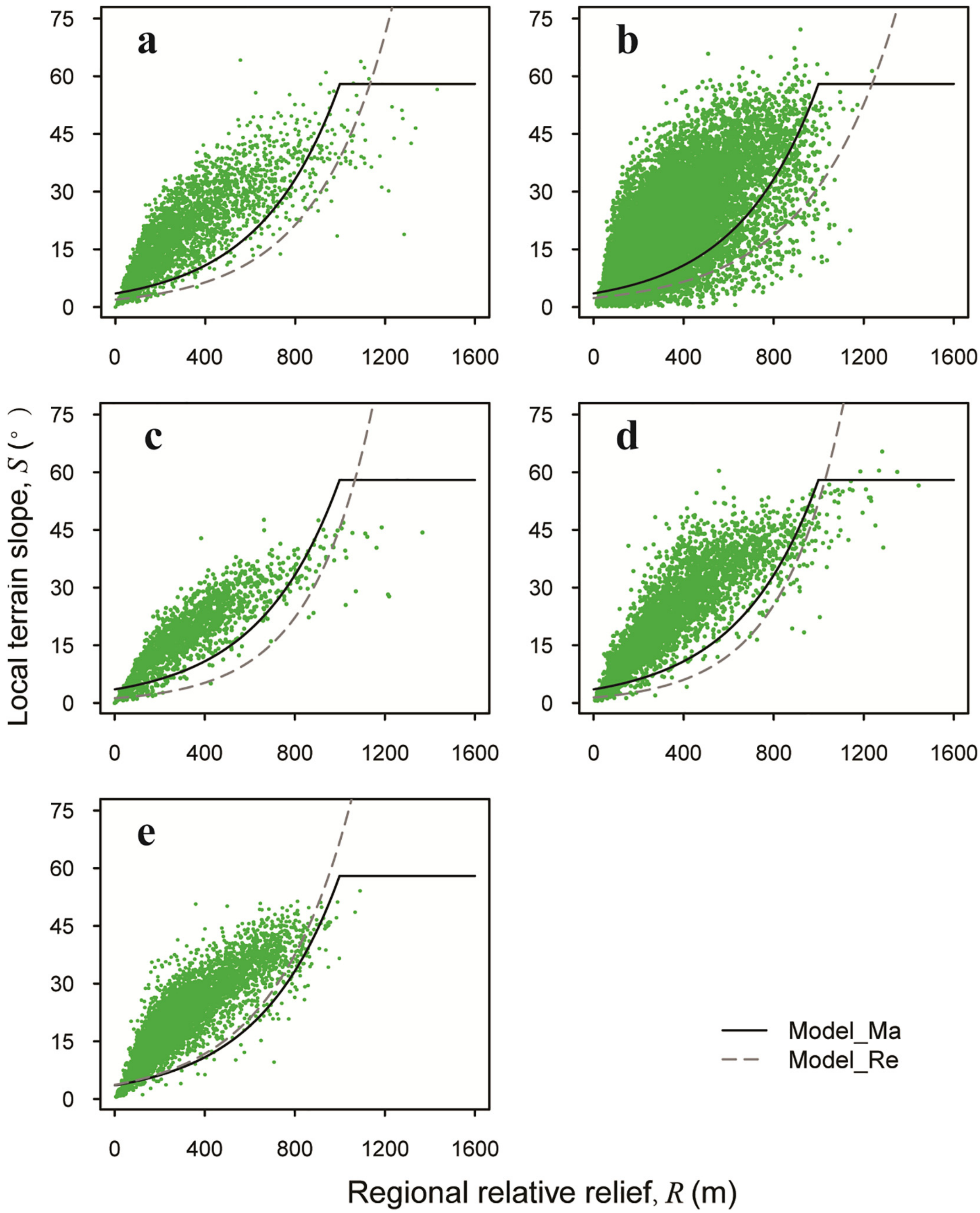

Fig. 7. Regional QNL non-susceptibility models based on the groups of landslide datasets. Model_Ma: QNL model proposed by Marchesini et al. (2014). Model_re: regional QNL models for (a) COOLR dataset, (b) Region B (grouped datasets in Fig. 1b), (c) Region C (grouped datasets in Fig. 1c), (d) Region D (grouped datasets in Fig. 1d), and (e) Region E (grouped datasets in Fig. 1e).

exist among models of different landslide types. The curve of complex landslides (Fig. 8e) is most similar to Model_Ma, while debris flows and mudslides give rise to lower minimum slope thresholds (Table 5). We concluded that the influence of geological and type factors cannot be ignored for further extending analyses of non-susceptibility, though the non-susceptibility models for different regions and landslide types in this study are not enough to conduct regional or global non-susceptibility analyses.

5. Conclusions

This study aimed at preparing a global landslide non-susceptibility map to highlight the areas where expected landslide susceptibility is null or negligible, by extending the model trained in Italy and applied to the Mediterranean region by Marchesini et al. (2014), with a maximum slope threshold of 58°. Non-susceptible areas were singled out by means of a relief-slope QNL threshold, with expected 5% misclassifications. Our findings are as follows:

1) The GLNSM (Fig. 5) obtained here covers 82.9% of global landmasses.
2) The QNL model proposed by Marchesini et al. (2014) shows good classification performance against global and regional datasets, with overall $FPR = 0.12$ (Table 2). Some regional landslide datasets (Fig. 3) and datasets grouped by landslide types (Table 2) score with lower *FPRs* (better performances) with respect to the global result. We maintain that the non-susceptibility model works well when uncertainty on landslide location is reduced.

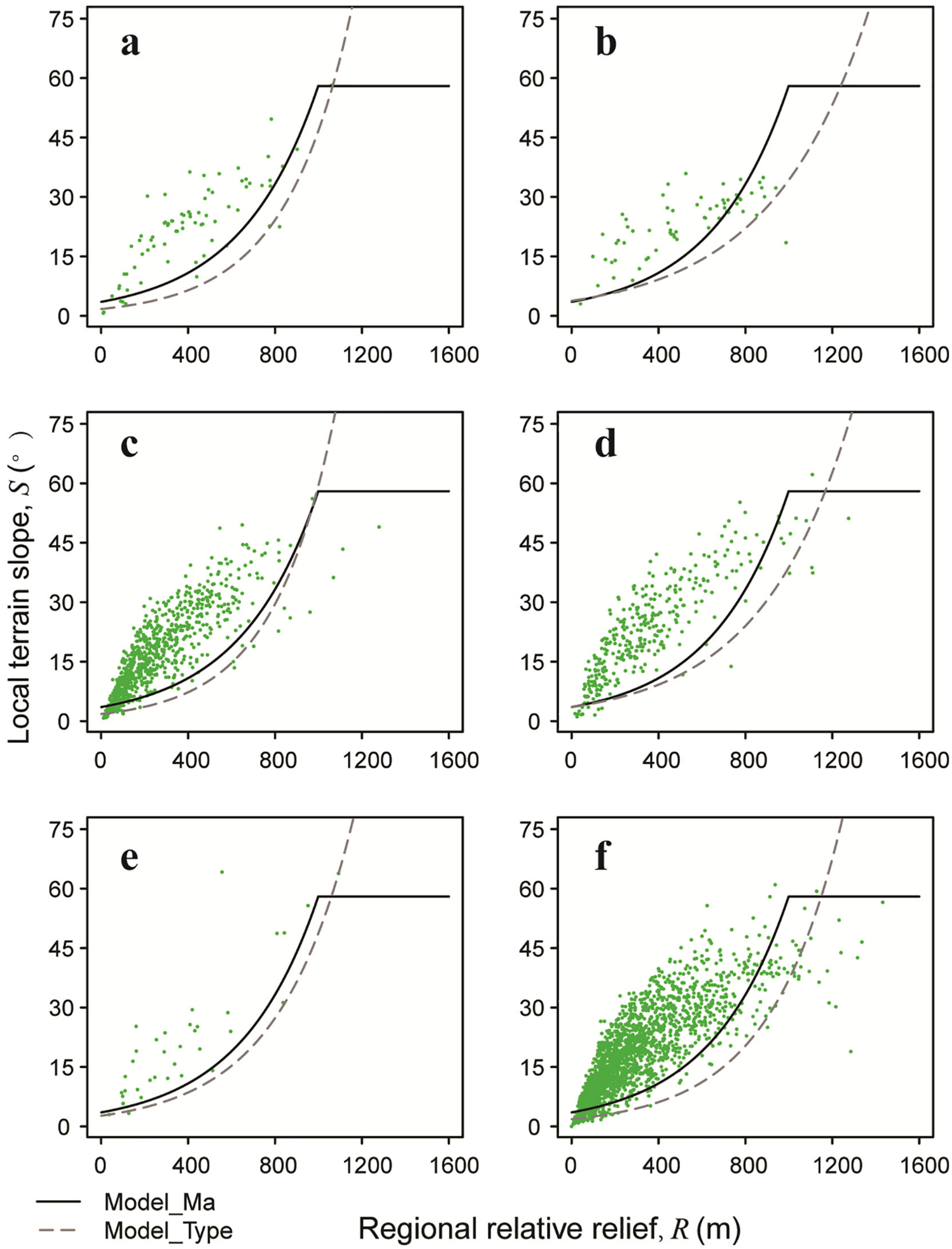

Fig. 8. QNL non-susceptibility models for different landslide types based on a global landslide dataset (COOLR). Model_Ma: QNL model proposed by Marchesini et al. (2014). Model_type: QNL models for landslide types of (a) debris flows, (b) translational/rotational slides, (c) mudslides, (d) rock falls, (e) complex landslides, and (f) others.

3) The GLNSM is generally consistent with the "very-low" susceptibility class in existing global and continental susceptibility maps (Table 3), and shares a similar spatial distribution with the national non-susceptibility map in the conterminous United States (Fig. 6).
4) The GLNSM is promising for decision-making in land planning and disaster responses. Globally, 91.8% of the population lives, and 91.2% of the settlements are located, in non-susceptible areas (Table 4). The population and built-up densities are significantly higher in non-susceptible areas compared with that outside the non-susceptible areas.
5) Non-susceptibility analyses are significantly influenced by landslide types (Fig. 8). Moreover, quantile models obtained in different regions (Fig. 7) are significantly different. This suggests that considering the variability of geological setting, and landslide type, is mandatory for further extending regional non-susceptibility analyses.

The GLNSM proposed in this work, or analogous local maps derived from higher-resolution DEMs, can be a useful tool to illustrate where the likelihood of landslide occurrence is zero or negligible. We suggest that the map can be used for a priori exclusion of non-susceptible areas from

Table 5
Parameters of QNL models for the globe and different regions corresponding to regional views in Fig. 1 and landslide types based on the COOLR dataset. The models are defined as Eq. (1) in Section 3.1. Datasets: Region B (grouped datasets in Fig. 1b), Region C (grouped datasets in Fig. 1c), Region D (grouped datasets in Fig. 1d), Region E (grouped datasets in Fig. 1e).

	Dataset	α	β
Regions	COOLR	1.938	0.0030
	Region B	2.326	0.0026
	Region C	1.246	0.0036
	Region D	1.431	0.0036
	Region E	3.686	0.0029
Landslide types	Debris flows	1.725	0.0033
	Translational/ rotational slides	3.800	0.0022
	Mudslides	1.796	0.0035
	Rock falls	3.521	0.0024
	Complex landslides	2.686	0.0029
	Others	1.846	0.0030

susceptibility zonation (Alvioli et al., 2016). Moreover, for landslide early warning systems, an easy-to-interpret map of areas with zero likelihood of landslide occurrence could simplify decision making, to focus on areas outside the non-susceptible areas. Indeed, the map of Marchesini et al. (2014) served to that purpose for national landslide warning system in Italy (Guzzetti et al., 2020). We maintain that our global map might be useful for a global knowledge of landslide hazard and risk assessment.

Declaration of competing interest

The authors declare that they have no known competing financial interests or personal relationships that could have appeared to influence the work reported in this paper.

Acknowledgements

This work is supported by the National Natural Science Foundation of China (Grant No. 41730645), the Strategic Priority Research Program of Chinese Academy of Sciences (Grant No. XDA20060402), and the Second Tibetan Plateau Scientific Expedition and Research (Grant No. 2019QZKK0208). G. Jia was supported by the China Scholarship Council (CSC201904910615) and acknowledged kind hospitality and support of CNR IRPI, Perugia. We further appreciated the three anonymous reviewers for their valuable comments, which helped us improve our work greatly.

Appendix A. Supplementary data

Supplementary data to this article can be found online at https://doi.org/10.1016/j.geomorph.2021.107804.

References

AGS, 2015. Natural Hazards in Arizona. Arizona Geological Survey. Available:. https://uagis.maps.arcgis.com/apps/webappviewer/index.html?id=98729f76e4644f1093d1c2cd6dabb584. (Accessed 18 December 2020).

Alvioli, M., Marchesini, I., Reichenbach, P., Rossi, M., Ardizzone, F., Fiorucci, F., Guzzetti, F., 2016. Automatic delineation of geomorphological slope units with r.slopeunits v1.0 and their optimization for landslide susceptibility modeling. Geosci. Model Dev. 9, 3975–3991. https://doi.org/10.5194/gmd-9-3975-2016.

Alvioli, M., Melillo, M., Guzzetti, F., Rossi, M., Palazzi, E., von Hardenberg, J., Brunetti, M.T., Peruccacci, S., 2018. Implications of climate change on landslide hazard in central Italy. Sci. Total Environ. 630, 1528–1543. https://doi.org/10.1016/j.scitotenv.2018.02.315.

Alvioli, M., Guzzetti, F., Marchesini, I., 2020. Parameter-free delineation of slope units and terrain subdivision of Italy. Geomorphology 358, 107124. https://doi.org/10.1016/j.geomorph.2020.107124.

Benz, S.A., Blum, P., 2019. Global detection of rainfall-triggered landslide clusters. Nat. Hazards Earth Syst. Sci. 19, 1433–1444. https://doi.org/10.5194/nhess-19-1433-2019.

Biasutti, M., Seager, R., Kirschbaum, D.B., 2016. Landslides in West Coast metropolitan areas: the role of extreme weather events. Weather Clim. Extrem. 14, 67–79. https://doi.org/10.1016/j.wace.2016.11.004.

Broeckx, J., Vanmaercke, M., Duchateau, R., Poesen, J., 2018. A data-based landslide susceptibility map of Africa. Earth Sci. Rev. 185, 102–121. https://doi.org/10.1016/j.earscirev.2018.05.002.

Budimir, M.E.A., Atkinson, P.M., Lewis, H.G., 2015. A systematic review of landslide probability mapping using logistic regression. Landslides 12, 419–436. https://doi.org/10.1007/s10346-014-0550-5.

Burns, W.J., Madin, I.P., 2009. Protocol for inventory mapping of landslide deposits from light detection and ranging (lidar) imagery. Oregon Department of Geology and Mineral Industries, Special Paper 42 https://digital.osl.state.or.us/islandora/object/osl%3A24647/datastream/OBJ/download/Protocol_for_inventory_mapping_of_landslide_deposits_from_light_detection_and_ranging__lidar__imagery.pdf.

Calvello, M., Pecoraro, G., 2018. FraneItalia: a catalog of recent Italian landslides. Geoenvironmental Disasters. 5, p. 13. https://doi.org/10.1186/s40677-018-0105-5.

Clift, A.E., Springston, G., 2012. Protocol for identification of areas sensitive to landslide hazards in Vermont. Vermont Geological Survey, Technical Report https://dec.vermont.gov/sites/dec/files/geo/TechReports/VGTR2012-1LandslideProtocol.pdf.

Cook, J.P., Pearthree, P.A., Gootee, B.F., Conway, B.D., Youberg, A., 2016. Landslides are surprisingly large and widespread in Arizona. Geological Society of America Annual Conference, Colorado, United States https://repository.arizona.edu/handle/10150/629611.

Creighton, R., 2006. Landslides in Ireland: A report of the Irish landslides working group. Geological Survey of Ireland, Technical Report https://www.gsi.ie/documents/Landslides_in_Ireland_2006.pdf.

Cruden, D.M., Varnes, D.J., 1996. Landslide types and processes. In: Turner, A.K., Schuster, R.L. (Eds.), Landslides: Investigation and Mitigation. National Academy Press, Washington DC, USA, pp. 1–77.

Dai, F.C., Lee, C.F., Ngai, Y.Y., 2002. Landslide risk assessment and management: An overview. Eng. Geol. 64, 65–87. https://doi.org/10.1016/S0013-7952(01)00093-X.

Elliott, A.H., Harty, K.M., 2010. Landslide Maps of Utah. Utah Geological Survey, Technical Report https://www.utahmapstore.com/collections/landslides/products/m-246?variant=32205592592437.

Farahmand, A., Aghakouchak, A., 2013. A satellite-based global landslide model. Nat. Hazards Earth Syst. Sci. 13, 1259–1267. https://doi.org/10.5194/nhess-13-1259-2013.

Florczyk, A.J., Corbane, C., Ehrlich, D., Freire, S., Kemper, T., Maffenini, L., Melchiorri, M., Pesaresi, M., Politis, P., Schiavina, M., Sabo, F., Zanchetta, L., 2019. GHSL Data Package 2019. Luxembourg. https://doi.org/10.2760/062975.

Froude, M.J., Petley, D.N., 2018. Global fatal landslide occurrence from 2004 to 2016. Nat. Hazards Earth Syst. Sci. 18, 2161–2181. https://doi.org/10.5194/nhess-18-2161-2018.

Gariano, S.L., Guzzetti, F., 2016. Landslides in a changing climate. Earth Sci. Rev. 162, 227–252. https://doi.org/10.1016/j.earscirev.2016.08.011.

GDDPMC, 2016. Yearbook of disaster prevention and mitigation in Guangdong, China. Guangdong Disaster Prevention and Mitigation Committee, Technical Report http://ss.zhizhen.com/detail_38502727e7500f262814f69715a39ba4e301f9b9028d38f41921b0a3ea25510134114c969f2eae5c12132a9ac61ae8899d230af272b6db831e76ddfdf533af545b1b44a1a422ad3ad80a977f299f2a8c?&apistrclassfy=0_21_8.

Geoscience Australia, 2012. Landslide Search. Canberra. Available:. http://pid.geoscience.gov.au/dataset/ga/74273. (Accessed 18 December 2020).

Giuliani, G., Peduzzi, P., 2011. The PREVIEW global risk data platform: a geoportal to serve and share global data on risk to natural hazards. Nat. Hazards Earth Syst. Sci. 11, 53–66. https://doi.org/10.5194/nhess-11-53-2011.

Godt, J.W., Coe, J.A., Baum, R.L., Highland, L.M., Keaton, J.R., Roth, R.J., 2012. Prototype landslide hazard map of the conterminous United States. In: Eberhardt, E., Froese, C., Leroueil, S., Turner, K. (Eds.), Landslides and Engineered Slopes: Protecting Society through Improved Understanding. Taylor & Francis Group, London, pp. 245–250.

Görüm, T., Fidan, S., 2021. Spatiotemporal variations of fatal landslides in Turkey (online). Landslides https://doi.org/10.1007/s10346-020-01580-7.

Guzzetti, F., Reichenbach, P., Cardinali, M., Galli, M., Ardizzone, F., 2005. Probabilistic landslide hazard assessment at the basin scale. Geomorphology 72, 272–299. https://doi.org/10.1016/j.geomorph.2005.06.002.

Guzzetti, F., Peruccacci, S., Rossi, M., Stark, C.P., 2008. The rainfall intensity-duration control of shallow landslides and debris flows: an update. Landslides 5, 3–17. https://doi.org/10.1007/s10346-007-0112-1.

Guzzetti, F., Mondini, A.C., Cardinali, M., Fiorucci, F., Santangelo, M., Chang, K.T., 2012. Landslide inventory maps: new tools for an old problem. Earth Sci. Rev. 112, 42–66. https://doi.org/10.1016/j.earscirev.2012.02.001.

Guzzetti, F., Gariano, S.L., Peruccacci, S., Brunetti, M.T., Marchesini, I., Rossi, M., Melillo, M., 2020. Geographical landslide early warning systems. Earth Sci. Rev. 200, 102973. https://doi.org/10.1016/j.earscirev.2019.102973.

Haque, U., da Silva, P.F., Devoli, G., Pilz, J., Zhao, B., Khaloua, A., Wilopo, W., Andersen, P., Lu, P., Lee, J., Yamamoto, T., Keellings, D., Wu, J., Glass, G.E., 2019. The human cost of global warming: deadly landslides and their triggers (1995-2014). Sci. Total Environ. 682, 673–684. https://doi.org/10.1016/j.scitotenv.2019.03.415.

Hong, Y., Adler, R.F., 2008. Predicting global landslide spatiotemporal distribution: Integrating landslide susceptibility zoning techniques and real-time satellite rainfall estimates. Int. J. Sediment Res. 23, 249–257. https://doi.org/10.1016/S1001-6279(08)60022-0.

Hong, Y., Alder, R.F., Huffman, G., 2006. Evaluation of the potential of NASA multi-satellite precipitation analysis in global landslide hazard assessment. Geophys. Res. Lett. 33, 1–5. https://doi.org/10.1029/2006GL028010.

Hong, Y., Adler, R.F., Huffman, G., 2007a. Use of satellite remote sensing data in the mapping of global landslide susceptibility. Nat. Hazards 43, 245–256. https://doi.org/10.1007/s11069-006-9104-z.

Hong, Y., Adler, R.F., Huffman, G., 2007b. An experimental global prediction system for rainfall-triggered landslides using satellite remote sensing and geospatial datasets. IEEE Trans. Geosci. Remote Sens. 45, 1671–1680. https://doi.org/10.1109/TGRS.2006.888436.
Huang, Y., Zhao, L., 2018. Review on landslide susceptibility mapping using support vector machines. Catena 165, 520–529. https://doi.org/10.1016/j.catena.2018.03.003.
Hungr, O., 2007. Dynamics of rapid landslides. In: Sassa, K., Fukuoka, H., Wang, F., Wang, G. (Eds.), Progress in Landslide Science. Springer, Berlin, Heidelberg, pp. 47–57 https://doi.org/10.1007/978-3-540-70965-7_4.
Jacobs, L., Kervyn, M., Reichenbach, P., Rossi, M., Marchesini, I., Alvioli, M., Dewitte, O., 2020. Regional susceptibility assessments with heterogeneous landslide information: slope unit- vs. pixel-based approach. Geomorphology 356, 107084. https://doi.org/10.1016/j.geomorph.2020.107084.
Jarvis, A., Reuter, H., Nelson, A., Guevara, E., 2008. Hole-filled SRTM for the Globe. CGIAR-CSI, v4. Available:. http://srtm.csi.cgiar.org. (Accessed 18 December 2020).
Jia, G., Tang, Q., Xu, X., 2020. Evaluating the performances of satellite-based rainfall data for global rainfall-induced landslide warnings. Landslides 17, 283–299. https://doi.org/10.1007/s10346-019-01277-6.
Juang, C.S., Stanley, T.A., Kirschbaum, D.B., 2019. Using citizen science to expand the global map of landslides: introducing the Cooperative Open Online Landslide Repository (COOLR). PLoS One 14, 1–28. https://doi.org/10.1371/journal.pone.0218657.
Kirschbaum, D.B., Stanley, T., 2018. Satellite-based assessment of rainfall-triggered landslide hazard for situational awareness. Earth's Futur. 6, 505–523. https://doi.org/10.1002/2017EF000715.
Kirschbaum, D.B., Adler, R.F., Hong, Y., Lerner-Lam, A., 2009. Evaluation of a preliminary satellite-based landslide hazard algorithm using global landslide inventories. Nat. Hazards Earth Syst. Sci. 9, 673–686. https://doi.org/10.5194/nhess-9-673-2009.
Kirschbaum, D.B., Adler, R.F., Hong, Y., Hill, S., Lerner-Lam, A., 2010. A global landslide catalog for hazard applications: method, results, and limitations. Nat. Hazards 52, 561–575. https://doi.org/10.1007/s11069-009-9401-4.
Kirschbaum, D.B., Stanley, T., Zhou, Y., 2015. Spatial and temporal analysis of a global landslide catalog. Geomorphology 249, 4–15. https://doi.org/10.1016/j.geomorph.2015.03.016.
Li, W., Liu, C., Hong, Y., Zhang, X., Wang, Z., Saharia, M., Sun, W., Yao, D., Chen, W., Chen, S., Yang, X., Yue, J., 2016. A public Cloud-based China's Landslide Inventory Database (CsLID): development, zone, and spatiotemporal analysis for significant historical events, 1949-2011. J. Mt. Sci. 13, 1275–1285. https://doi.org/10.1107/s11629-015-3659-7.
Lin, L., Lin, Q., Wang, Y., 2017. Landslide susceptibility mapping on a global scale using the method of logistic regression. Nat. Hazards Earth Syst. Sci. 17, 1411–1424. https://doi.org/10.5194/nhess-17-1411-2017.
Marchesini, I., Ardizzone, F., Alvioli, M., Rossi, M., Guzzetti, F., 2014. Non-susceptible landslide areas in Italy and in the Mediterranean region. Nat. Hazards Earth Syst. Sci. 14, 2215–2231. https://doi.org/10.5194/nhess-14-2215-2014.
Mazengarb, C., Stevenson, M., 2010. Tasmanian landslide map series: user guide and technical methodology. Tasmanian Geological Survey, Technical Report https://www.mrt.tas.gov.au/mrtdoc/dominfo/download/UR2010_01/UR2010_01.pdf.
McKeon, C., 2016. National landslide susceptibility mapping project summary. Geological Survey Ireland, Technical Report https://www.gsi.ie/documents/National_Sus_Map_Summary_FINAL_NEW.pdf.
Nadim, F., Kjekstad, O., Peduzzi, P., Herold, C., Jaedicke, C., 2006. Global landslide and avalanche hotspots. Landslides 3, 159–173. https://doi.org/10.1007/s10346-006-0036-1.
Nadim, F., Jaedicke, C., Smebye, H., Kalsnes, B., 2013. Assessment of global landslide hazard hotspots. In: Sassa, K., Rouhban, B., Briceno, S., McSaveney, M., He, B. (Eds.), Landslides: Global Risk Preparedness. Springer-Verlag, Berlin, Heidelberg, pp. 59–71 https://doi.org/10.1007/978-3-642-22087-6_4.
Osuchowski, M., Atkinson, R., 2008. Connecting diverse landslide inventories for improved information in Australia. Proceedings of the 1st World Landslide Forum, Tokyo, Japan, 18–21 November 2008.
Peruccacci, S., Brunetti, M.T., Gariano, S.L., Melillo, M., Rossi, M., Guzzetti, F., 2017. Rainfall thresholds for possible landslide occurrence in Italy. Geomorphology 290, 39–57. https://doi.org/10.1016/j.geomorph.2017.03.031.
Petley, D., Froude, M., 2019. Guide to the Global Fatal Landslide Database on ArcGIS Online (Version 2). Available:. https://drive.google.com/drive/folders/1kxUSXBl10OHPrGXIur6bM4PBoKX0C_LY. (Accessed 18 December 2020).
Reichenbach, P., Rossi, M., Malamud, B.D., Mihir, M., Guzzetti, F., 2018. A review of statistically-based landslide susceptibility models. Earth Sci. Rev. 180, 60–91. https://doi.org/10.1016/j.earscirev.2018.03.001.
Reuter, H., Nelson, A., Jarvis, A., 2007. An evaluation of void filling interpolation methods for SRTM data. Int. J. Geogr. Inf. Sci. 21, 983–1008. https://doi.org/10.1080/13658810601169899.
Rickenmann, D., 2005. Runout prediction methods. In: Jakob, M., Hungr, O. (Eds.), Debris-flow Hazards and Related Phenomena. Springer, Berlin, Heidelberg, pp. 305–324 https://doi.org/10.1007/3-540-27129-5_13.
Rosser, B., Dellow, S., Haubrock, S., Glassey, P., 2017. New Zealand's national landslide database. Landslides 14, 1949–1959. https://doi.org/10.1007/s10346-017-0843-6.
Sayre, R., Frye, C., Karagulle, D., Krauer, J., Breyer, S., Aniello, P., Wright, D.J., Payne, D., Adler, C., Warner, H., VanSistine, D.P., Cress, J., 2018. A new high-resolution map of world mountains and an online tool for visualizing and comparing characterizations of global mountain distributions. Mt. Res. Dev. 38, 240–249. https://doi.org/10.1659/mrd-journal-d-17-00107.1.
Slaughter, S.L., Burns, W.J., Mickelson, K.A., Jacobacci, K.E., Biel, A., Contreras, T.A., 2017. Protocol for landslide inventory mapping from lidar data in Washington state. Washington Geological Survey Bulletin 82 http://www.dnr.wa.gov/Publications/ger_b82_landslide_inventory_mapping_protocol.zip.
Stanley, T., Kirschbaum, D.B., 2017. A heuristic approach to global landslide susceptibility mapping. Nat. Hazards 87, 145–164. https://doi.org/10.1007/s11069-017-2757-y.
Tanyas, H., Lombardo, L., 2020. Completeness index for earthquake-induced landslide inventories. Eng. Geol. 264, 105331. https://doi.org/10.1016/j.enggeo.2019.105331.
Tanyas, H., Rossi, M., Alvioli, M., van Westen, C.J., Marchesini, I., 2019a. A global slope unit-based method for the near real-time prediction of earthquake-induced landslides. Geomorphology 327, 126–146. https://doi.org/10.1016/j.geomorph.2018.10.022.
Tanyas, H., van Westen, C.J., Persello, C., Alvioli, M., 2019b. Rapid prediction of the magnitude scale of landslide events triggered by an earthquake. Landslides 16, 661–676. https://doi.org/10.1007/s10346-019-01136-4.
Trigila, A., Iadanza, C., Spizzichino, D., 2010. Quality assessment of the Italian Landslide Inventory using GIS processing. Landslides 7, 455–470. https://doi.org/10.1007/s10346-010-0213-0.
UGS, 2018. Landslides and debris flows. Utah Geological Survey Available:. https://gis.utah.gov/data/geoscience/landslides/. (Accessed 18 December 2020).
USGS, 2020. Landslide Hazards. United States Geological Survey. Available:. https://www.usgs.gov/natural-hazards/landslide-hazards. (Accessed 18 December 2020).
Van Den Eeckhaut, M., Hervás, J., 2012. State of the art of national landslide databases in Europe and their potential for assessing landslide susceptibility, hazard and risk. Geomorphology 139-140, 545–558. https://doi.org/10.1016/j.geomorph.2011.12.006.
Van Den Eeckhaut, M., Hervás, J., Jaedicke, C., Malet, J.P., Montanarella, L., Nadim, F., 2012. Statistical modelling of Europe-wide landslide susceptibility using limited landslide inventory data. Landslides 9, 357–369. https://doi.org/10.1007/s10346-011-0299-z.
WGS, 2020. Landslide protocol inventory mapping—GIS data, February, 2020. Washington Geological Survey Digital Data Series 19, Version 2.0 https://fortress.wa.gov/dnr/geologydata/publications/data_download/ger_portal_landslide_inventory.zip.
Wilde, M., Günther, A., Reichenbach, P., Malet, J.P., Hervás, J., 2018. Pan-European landslide susceptibility mapping: ELSUS version 2. J. Maps 14, 97–104. https://doi.org/10.1080/17445647.2018.1432511.
YNDPMC, 2016. Yearbook of disaster prevention and mitigation in Yunnan, China. Yunnan Disaster Prevention and Mitigation Committee, Technical Report http://ss.zhizhen.com/detail_38502727e7500f268f2766febf6686c44c842e57df4519051921b0a3ea25510134114c969f2eae5cd616e9cc3373a273a0e2ec07cd17b56351cc4e29623d58fdb5465aecc36b7b3bbd319923364c989b.